Supporting Information for

A Generalized Strategy for Synthesizing Crystalline Bismuth-containing Nanomaterials

Liping Zhang, [a] Alexandre A. S. Gonçalves, [a] Baojiang Jiang [b] and Mietek Jaroniec *[a]

[a] Department of Chemistry and Biochemistry, Kent State University, Kent, Ohio 44242, USA

[b] School of Chemistry and Materials Science, Heilongjiang University, Harbin, Heilongjiang 150080, P. R. China.

Table S1. Chemicals used for the synthesis

Name	**Manufacturer**
Polyethylene glycol [PEG, $H(OCH_2CH_2)_nOH$, 7000 – 9000 g/mol]	Spectrum Chemical MFG Corp
Bismuth nitrate pentahydrate [$Bi(NO_3)_3{\cdot}5H_2O$]	Acros
Pluronic P123 [$H(OCH_2CH_2)_{20}(OCH(CH_3)CH_2)_{70}(OCH_2CH_2)_{20}OH$, ~5750 g/mol]	BASF
Pluronic F127 [$H(OCH_2CH_2)_{101}(OCH(CH_3)CH_2)_{56}(OCH_2CH_2)_{101}OH$, ~12600 g/mol]	BASF
Sodium orthorvanadate (Na_3VO_4)	Acros Organics
Potassium dichromate ($K_2Cr_2O_7$)	Fisher Scientific
Sodium molybdate dehydrate ($Na_2MoO_4{\cdot}2H_2O$)	Fisher Scientific
Sodium tungstate dehydrate ($Na_2WO_4{\cdot}2H_2O$)	J. T. Baker Chemical Co.
Potassium chloride (KCl)	Fisher Scientific
Potassium bromide (KBr)	Acros
Potassium iodide (KI)	Fisher Scientific
Sodium hydroxide (NaOH)	Acros
Copper sulfate anhydrous ($CuSO_4$)	Fisher Scientific
L-Ascorbic acid ($C_6H_8O_6$)	Sigma-Aldrich

Table S2. Identity and amount of polymers and precipitating agents used

Material	Polymer aqueous solution			Precipitating agent			Bi/(M + X)[a]
	Name	Conc. (mmol/L)	Volume (mL)	Formula	Mass (g)	Volume (mL)	
Bi_2O_3-PEG	PEG	5.0	25.0	NaOH	/	/	/
$BiVO_4$-PEG	PEG	5.0	25.0	Na_3VO_4	0.0460	25.0	1
$BiVO_4$-P123	P123	5.0	25.0	Na_3VO_4	0.0460	25.0	1
$BiVO_4$-F127	F127	5.0	25.0	Na_3VO_4	0.0460	25.0	1
$Bi_xCr_xO_z$-PEG	PEG	5.0	25.0	$K_2Cr_2O_7$	0.0368	25.0	1
$Bi_2Mo_2O_9$-PEG	PEG	5.0	25.0	$Na_2MoO_4{\cdot}2H_2O$	0.0605	25.0	1
Bi_2MoO_6-PEG	PEG	5.0	25.0	$Na_2MoO_4{\cdot}2H_2O$	0.0302	25.0	2
Bi_2WO_6-PEG	PEG	5.0	25.0	$Na_2WO_4{\cdot}2H_2O$	0.0412	25.0	2
BiOCl-PEG	PEG	5.0	25.0	KCl	0.0186	/	1
BiOBr-PEG	PEG	5.0	25.0	KBr	0.0298	/	1
BiOBr-P123	P123	5.0	25.0	KBr	0.0298	/	1
BiOI-PEG	PEG	5.0	25.0	KI	0.0415	/	1
BiOI-P123	P123	5.0	25.0	KI	0.0415	/	1
$BiVO_4$-BiOI-PEG	PEG	5.0	25.0	Na_3VO_4 + KI	0.0230 + 0.0208	25.0	1
$BiVO_4$-BiOBr-BiOI-PEG	PEG	5.0	25.0	Na_3VO_4 + KBr + KI	0.0153 + 0.0100 + 0.0138	25.0	1

[a]Molar ratio; M = V, Cr, Mo, or W; X = Cl, Br, or I.

Characterization

X-ray diffraction (XRD) was conducted on a MiniFlex 600 X-ray diffractometer (Rigaku Corporation, Tokyo, Japan) operating at a voltage and current of 40 kV and 15 mA, respectively. Energy-dispersive X-ray spectroscopy (EDX),

transmission electron microscopy (TEM) and scanning transmission electron microscopy (STEM) were performed on a FEI Tecnai G2 F20 Transmission Electron Microscope at a working voltage of 200 kV. Scanning electron microscopy (SEM) was carried out on a FEI Quanta 450 FEG Environmental Scanning Electron Microscope. UV-vis diffuse reflectance spectroscopy was performed on a Shimadzu UV-3600 Plus spectrophotometer with barium sulfate as the reference and calibration material.

Calculation

First, crystals were built based on the cell parameters calculated from XRD data and fractional coordinates retrieved from the Inorganic Crystal Structure Database (ICSD) (Table S3). The accuracy of the created crystal structures was confirmed by the fact that the simulated XRD patterns match well with the experimental patterns (Fig. S15). Density functional theory (DFT) calculations were carried out by using the Cambridge Serial Total Energy Package (CASTEP) on Materials Studio [1]. The Perdew-Burke-Ernzerhof (PBE) generalized gradient approximation (GGA) functional for solids (GGA-PBEsol) [2] was employed for both geometry optimization and density of states (DoS) calculation. During the geometry optimization using the Broyden-Fletcher-Goldfarb-Shanno (BFGS) scheme [3], convergence thresholds for energy, maximum force, stress, and displacement were set as 5.0×10^{-6} eV/atom, 0.01 eV/Å, 0.02 GPa, and 5.0×10^{-4} Å, respectively. For DoS calculations, the cutoff energy of plane wave basis set was 380.0 eV, and self-consistent filed (SCF) convergence threshold was 5.0×10^{-7} eV/atom.

Table S3. Cell parameters of Bi_2O_3, $Bi_xM_yO_z$, and BiOX and ICSD files used

Material	Lattice parameters[a]			ICSD entry
	a (Å)	*b* (Å)	*c* (Å)	
Bi_2O_3-PEG	5.85	8.17	7.51	94231
$BiVO_4$-PEG-400	5.31	5.16	11.98	33243
Bi_2MoO_6-PEG-400	5.50	16.22	5.51	47139
$Bi_2Mo_2O_9$-PEG-400	11.98	10.80	11.90	201742
Bi_2WO_6-PEG-400	5.45	16.52	5.38	67647
BiOCl-PEG	3.89	3.89	7.38	74502
BiOBr-PEG	3.85	3.85	8.20	61225
BiOI-PEG	4.00	4.00	9.15	391354

[a]Determined by XRD.

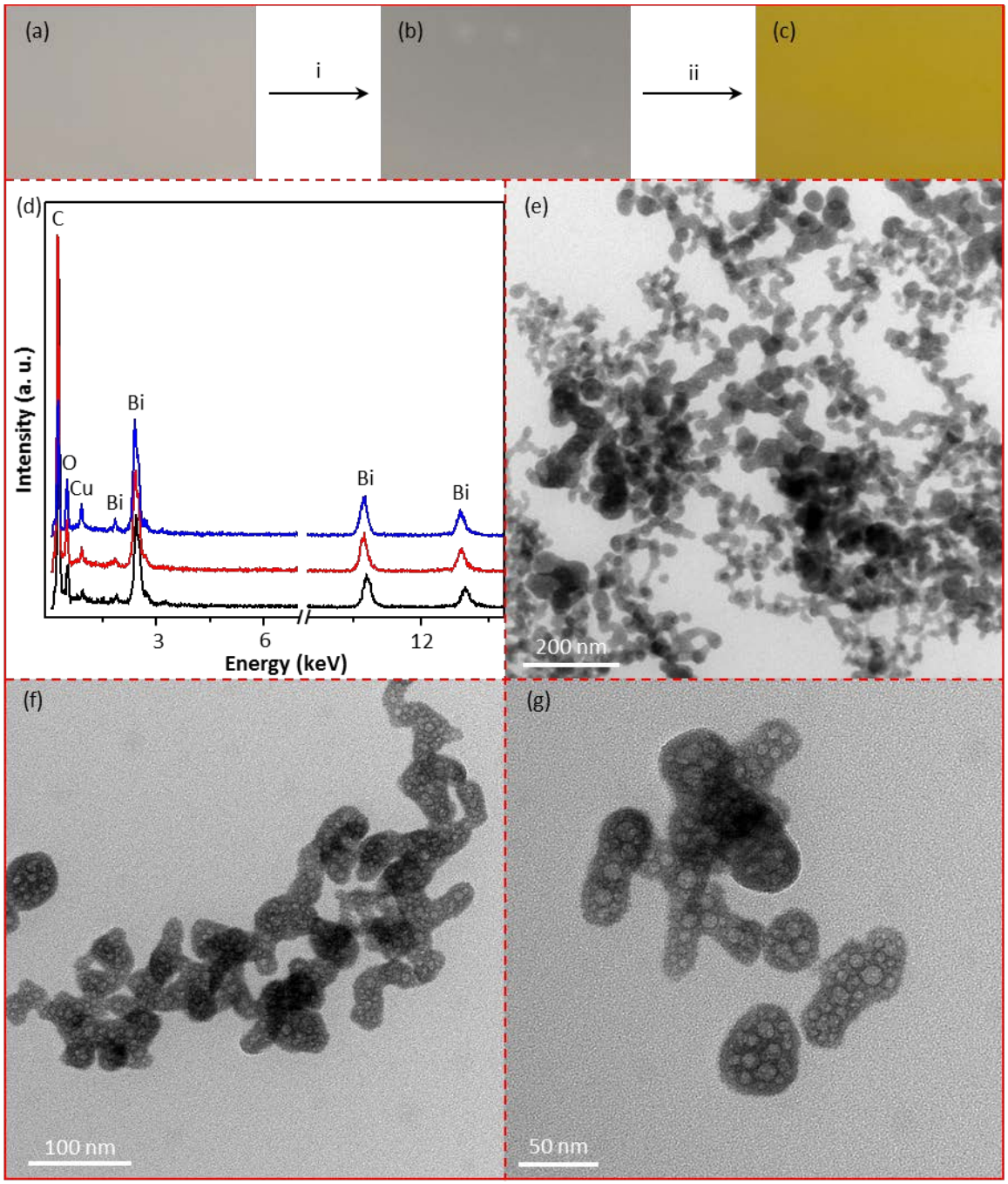

Fig. S1 Physical appearance of the aqueous suspension/solution(s) of (a) $Bi(NO_3)_3$, (b) $Bi(NO_3)_3$-polymer, and (c) $BiVO_4$-polymer, (d) EDX spectra and (e-g) TEM images of $Bi(NO_3)_3$-PEG-P123-HT.

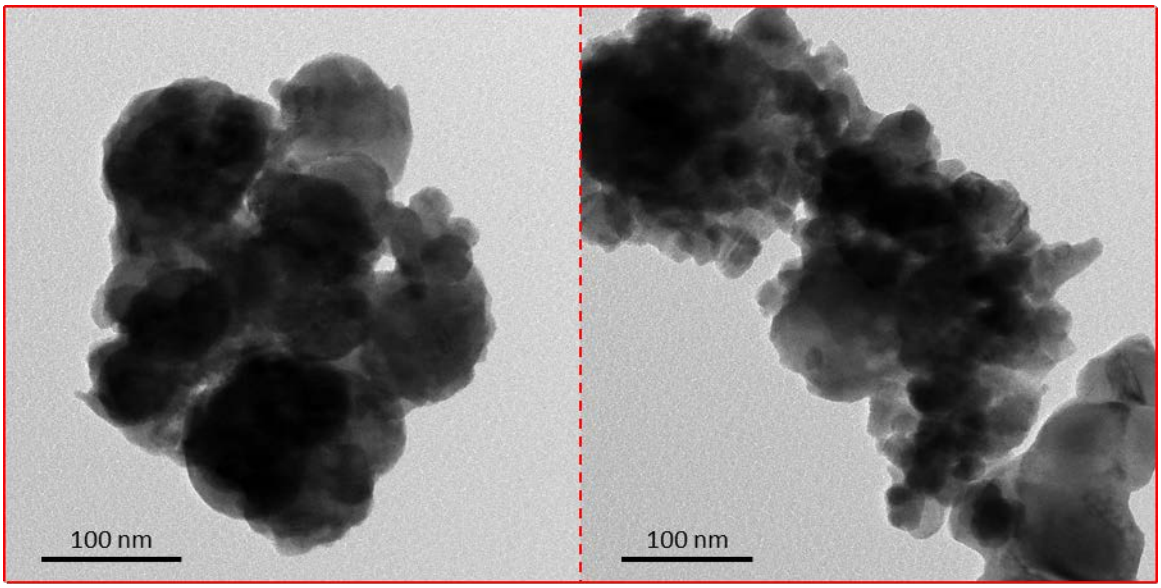

Fig. S2 TEM images of Bi_2O_3-PEG-P123-HT-400.

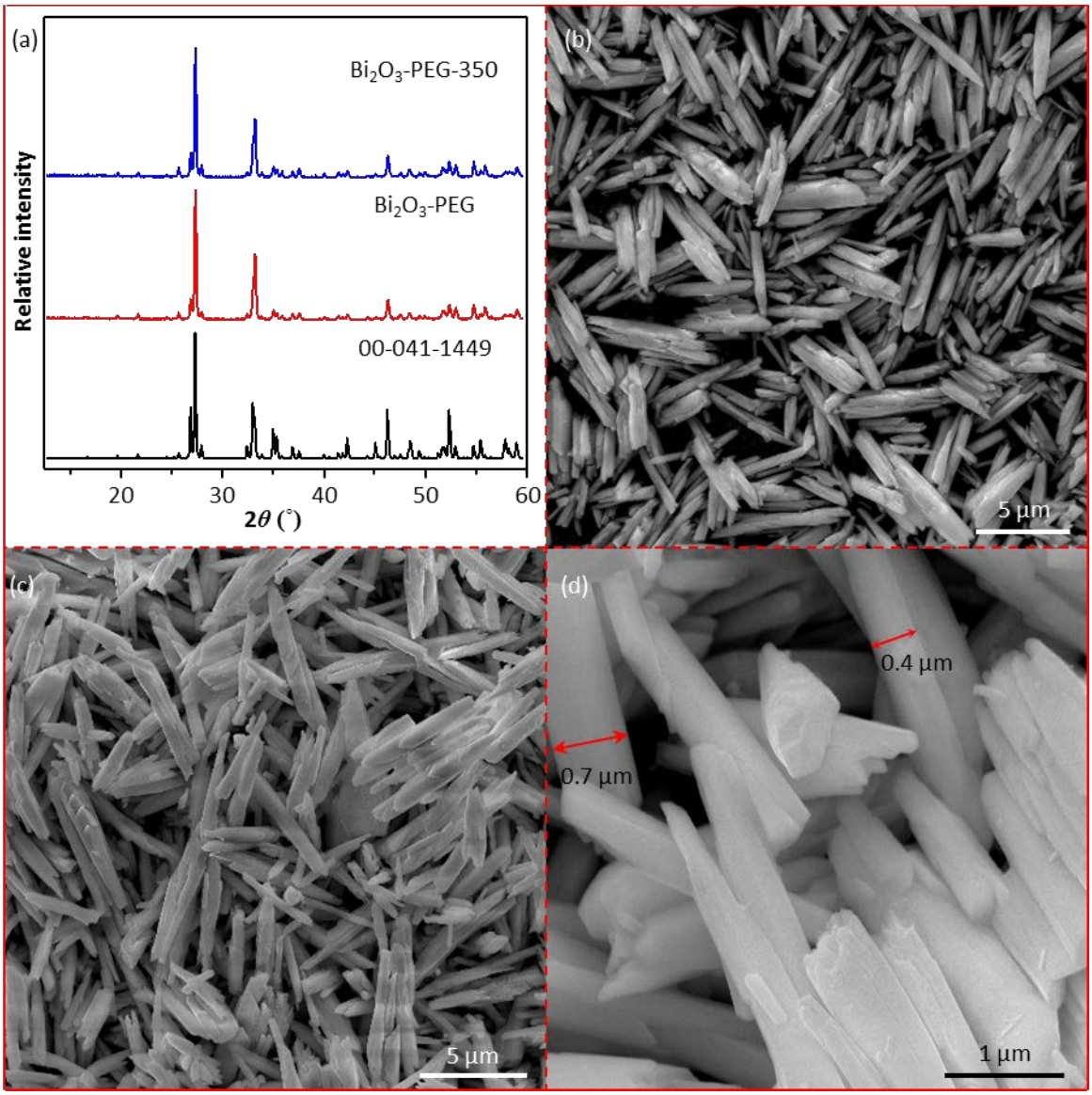

Fig. S3 (a) XRD patterns and SEM images of (b) Bi_2O_3-PEG and (c, d) Bi_2O_3-PEG-350.

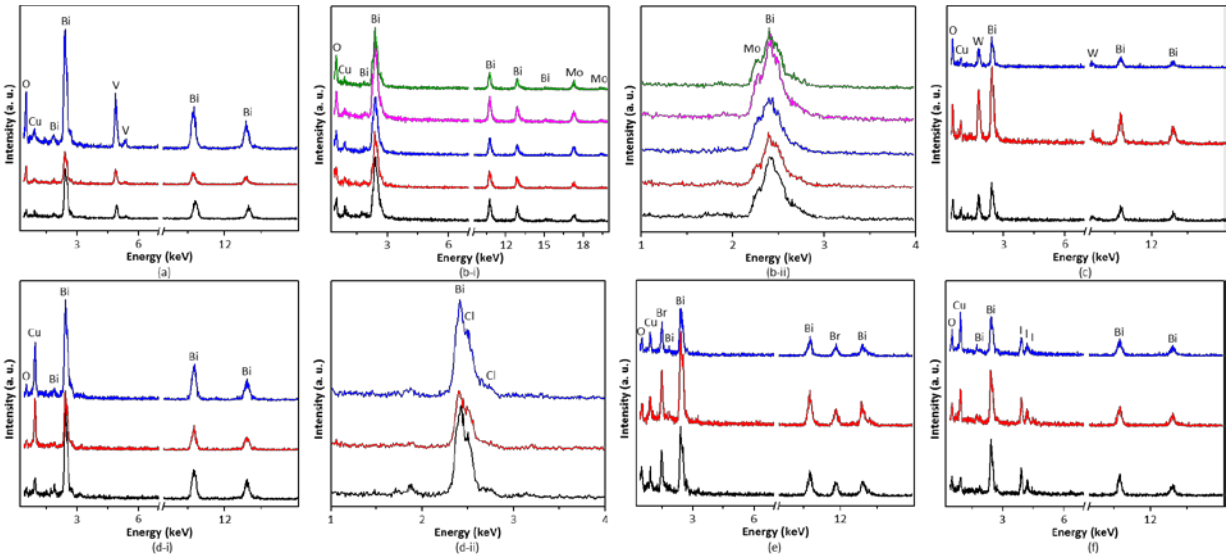

Fig. S4 EDX spectra of (a) $BiVO_4$-PEG, (b) $Bi_2Mo_2O_9$-PEG, (c) Bi_2WO_6-PEG, (d) BiOCl-PEG, (e) BiOBr-PEG, and (f) BiOI-PEG.

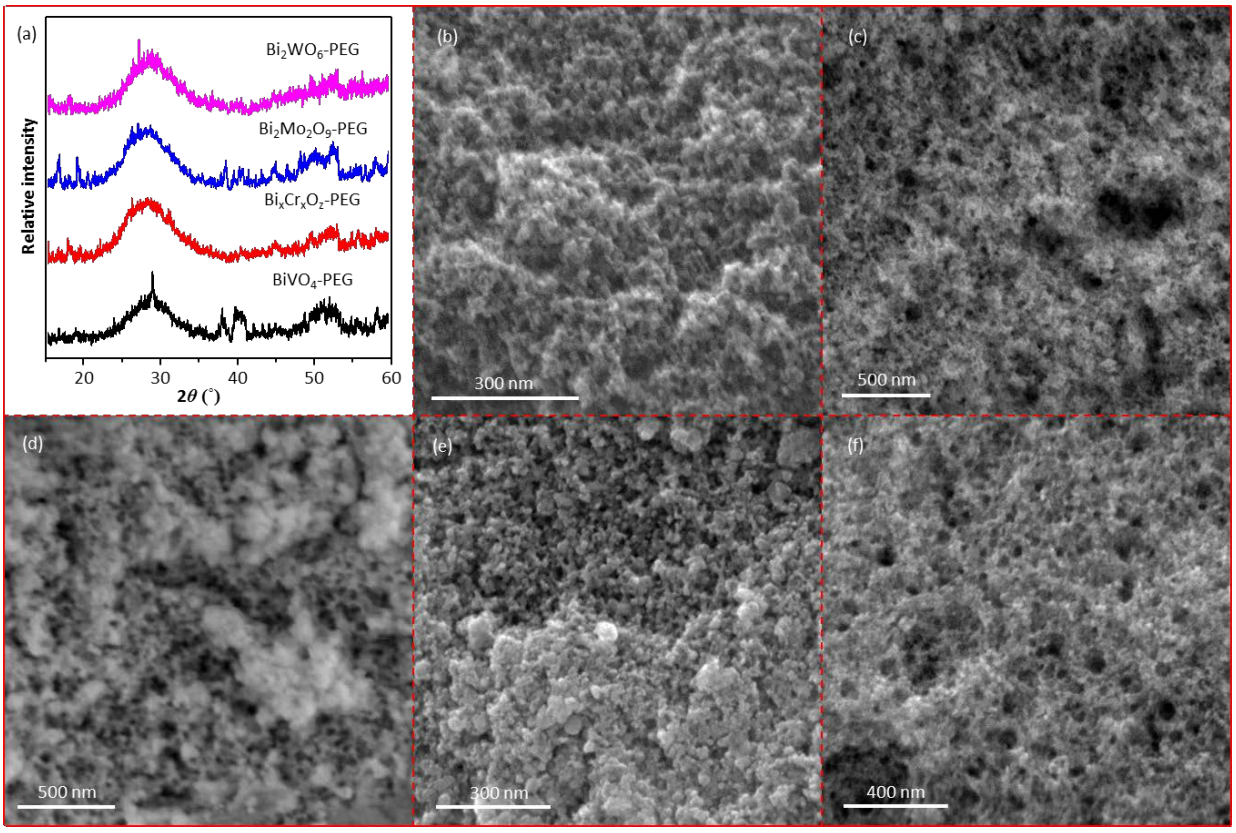

Fig. S5 (a) XRD patterns of $Bi_xM_yO_z$-PEG, SEM images of (b) $BiVO_4$-PEG, (c) $Bi_xCr_xO_z$-PEG, (d) Bi_2MoO_6-PEG, (e) $Bi_2Mo_2O_9$-PEG, and (f) Bi_2WO_6-PEG.

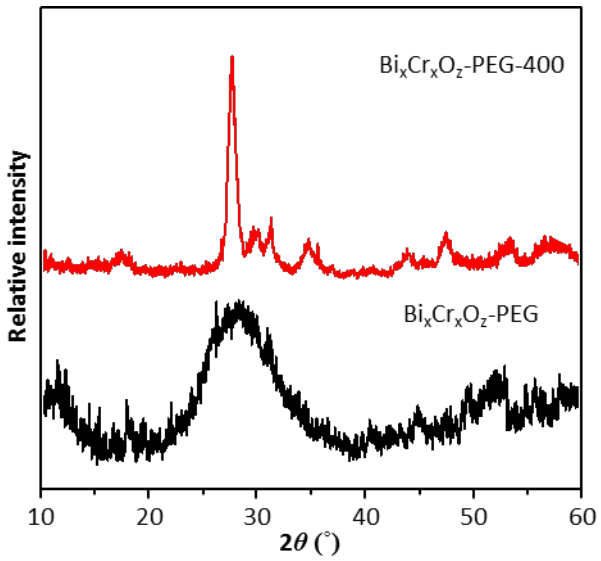

Fig. S6 XRD patterns of $Bi_xCr_xO_z$-PEG and $Bi_xCr_xO_z$-PEG-400.

As can be seen, $Bi_xCr_xO_z$-PEG-400 that has equal number of moles of Bi and Cr is also crystalline. Although, the XRD pattern could not be indexed, the demonstration of the synthetic strategy is not affected.

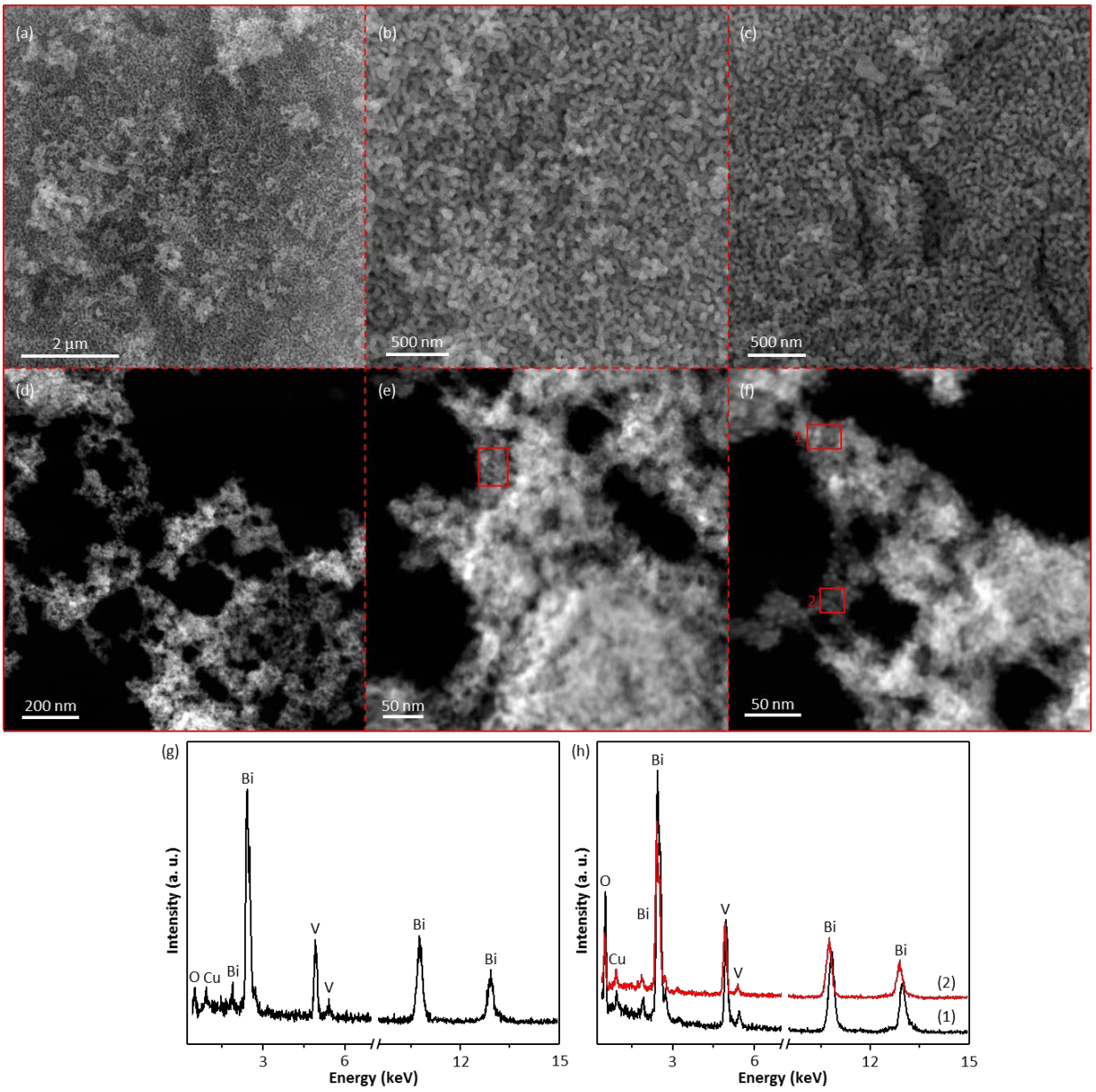

Fig. S7 (a-c) SEM images of $BiVO_4$-PEG-400, (d-f) STEM images of $BiVO_4$-PEG, and (g) and (h) corresponding EDX spectra recorded in the red frame-enclosed regions of (e) and (f), respectively.

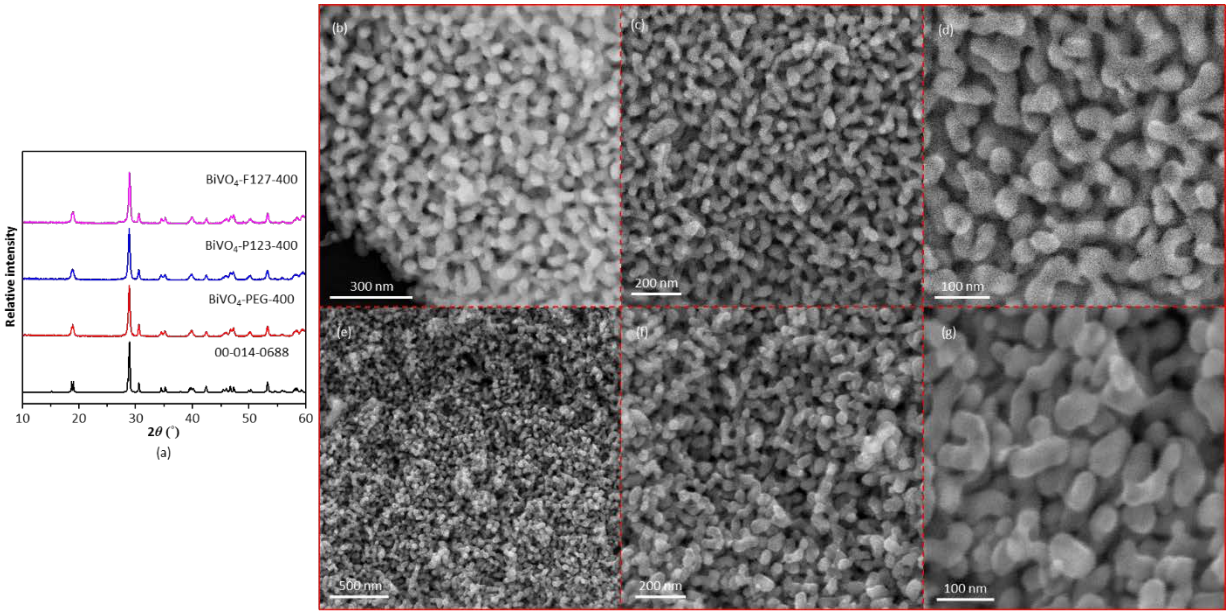

Fig. S8 (a) XRD patterns of $BiVO_4$-polymer-400, SEM images of (b-d) $BiVO_4$-P123-400 and (e-g) $BiVO_4$-F127-400.

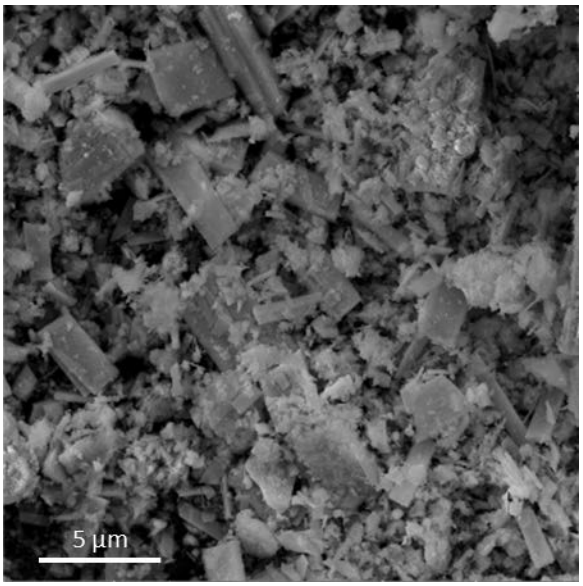

Fig. S9 SEM image of $BiVO_4$.

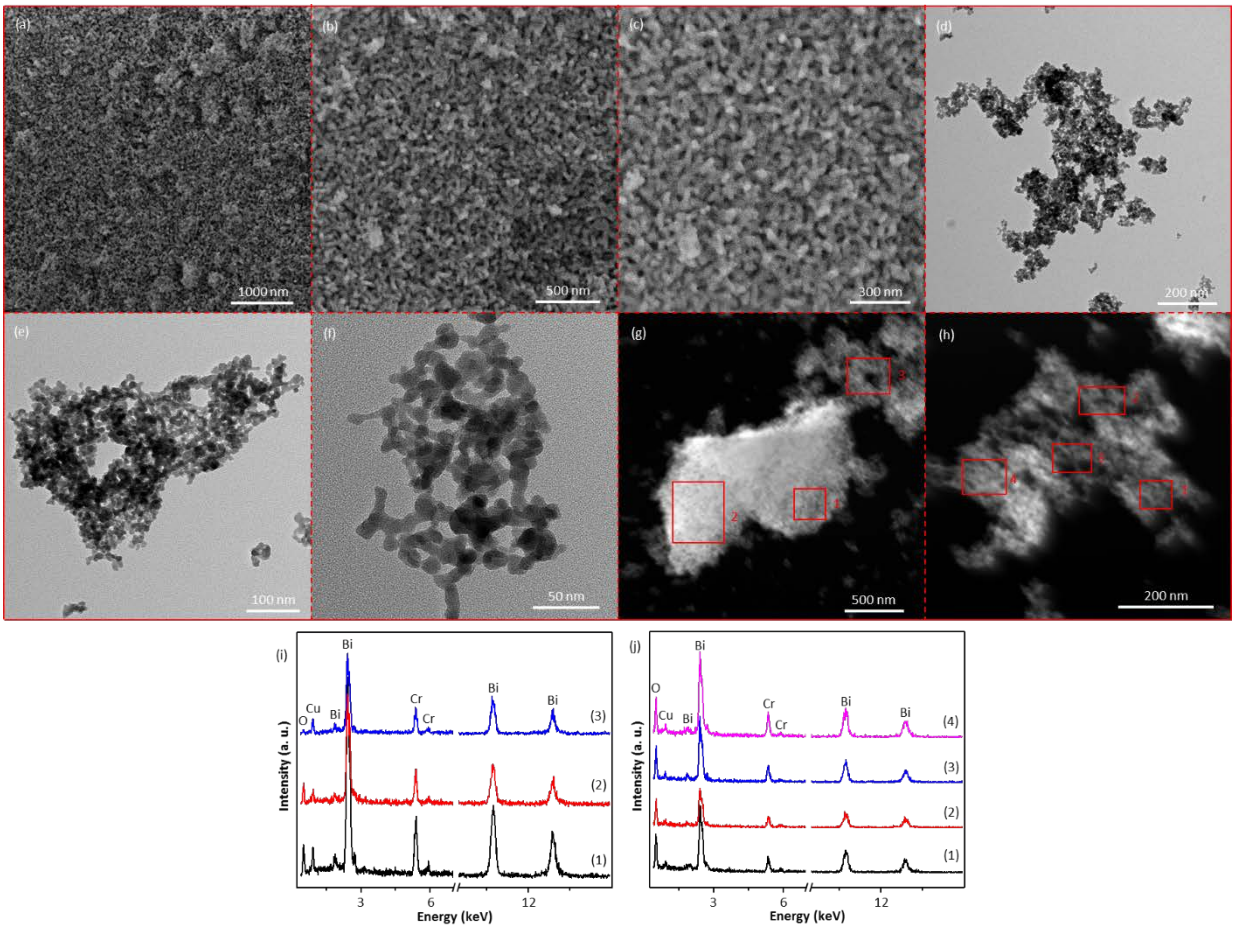

Fig. S10 (a-c) SEM images of $Bi_xCr_xO_z$-PEG-400, (d-f) TEM and (g, h) STEM images of $Bi_xCr_xO_z$-PEG, (i) and (j) corresponding EDX spectra recorded in the red frame-enclosed regions of (g) and (h), respectively.

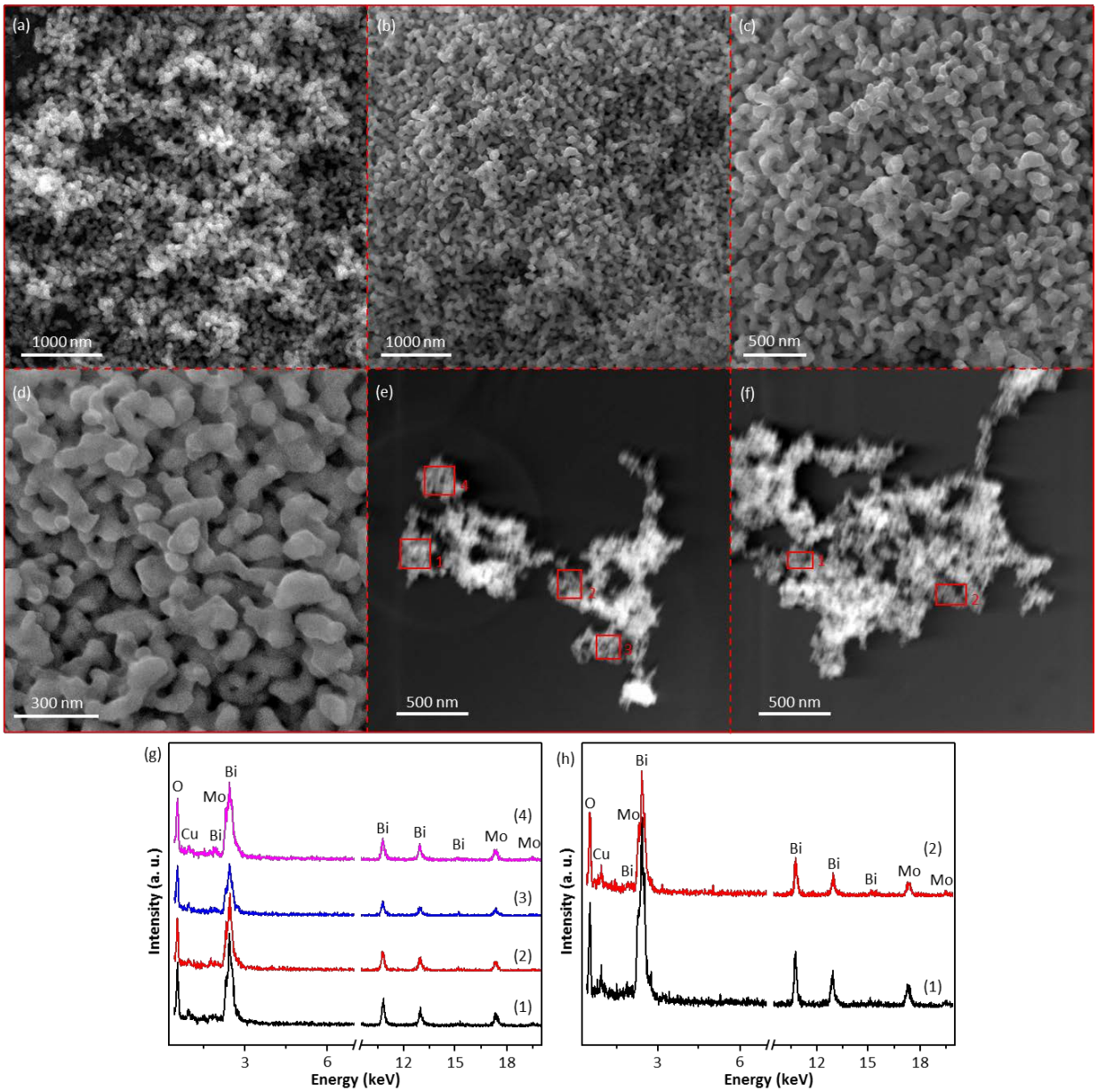

Fig. S11 (a-d) SEM images of $Bi_2Mo_2O_9$-PEG-400, (e-f) STEM images of $Bi_2Mo_2O_9$-PEG, and (g) and (h) corresponding EDX spectra recorded in the red frame-enclosed regions of (e) and (f), respectively.

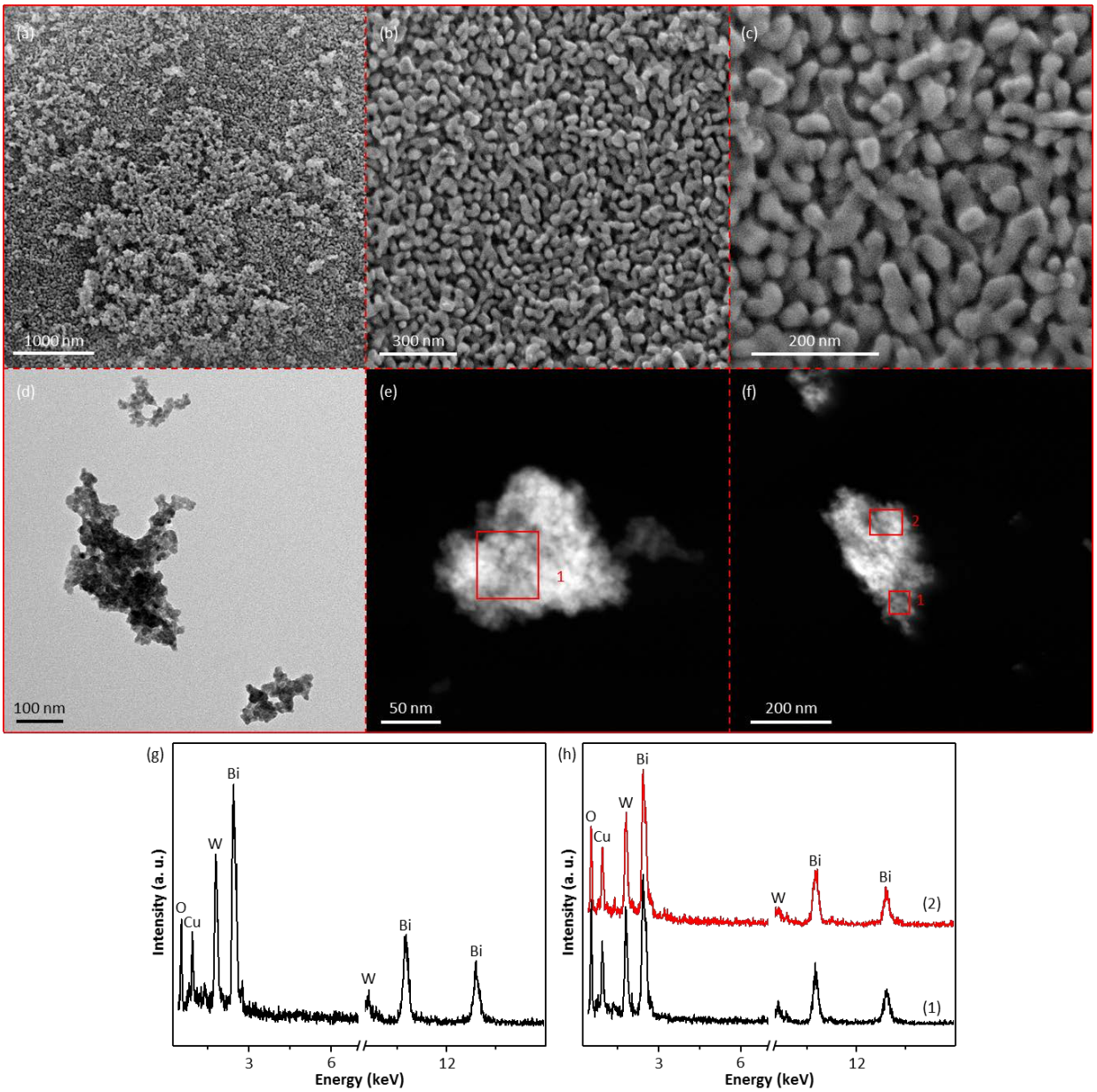

Fig. S12 (a-c) SEM images of Bi_2WO_6-PEG-400, (d) TEM and (e, f) STEM images of Bi_2WO_6-PEG, and (g) and (h) corresponding EDX spectra recorded in the red frame-enclosed regions of (e) and (f), respectively.

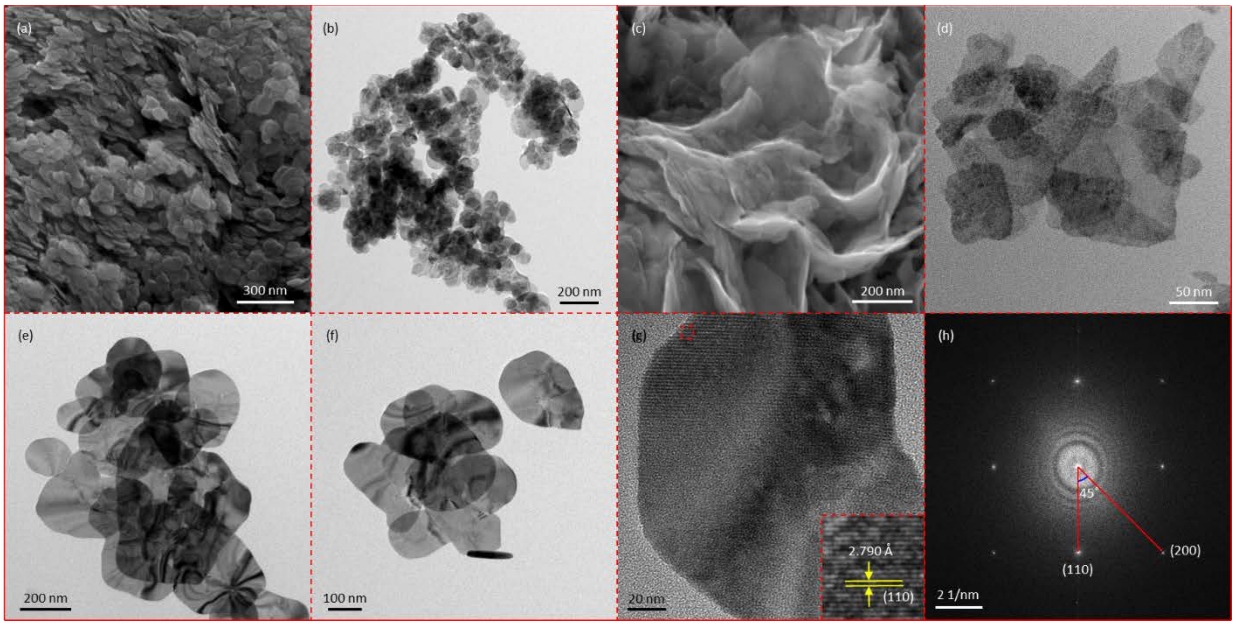

Fig. S13 (a) SEM and (b) TEM images of BiOCl-PEG, (c) SEM and (d) TEM images of BiOBr-PEG, (e-g) TEM images of BiOI-PEG (Insert is an enlargement of the red frame-enclosed area), (h) fast Fourier transform of (g).

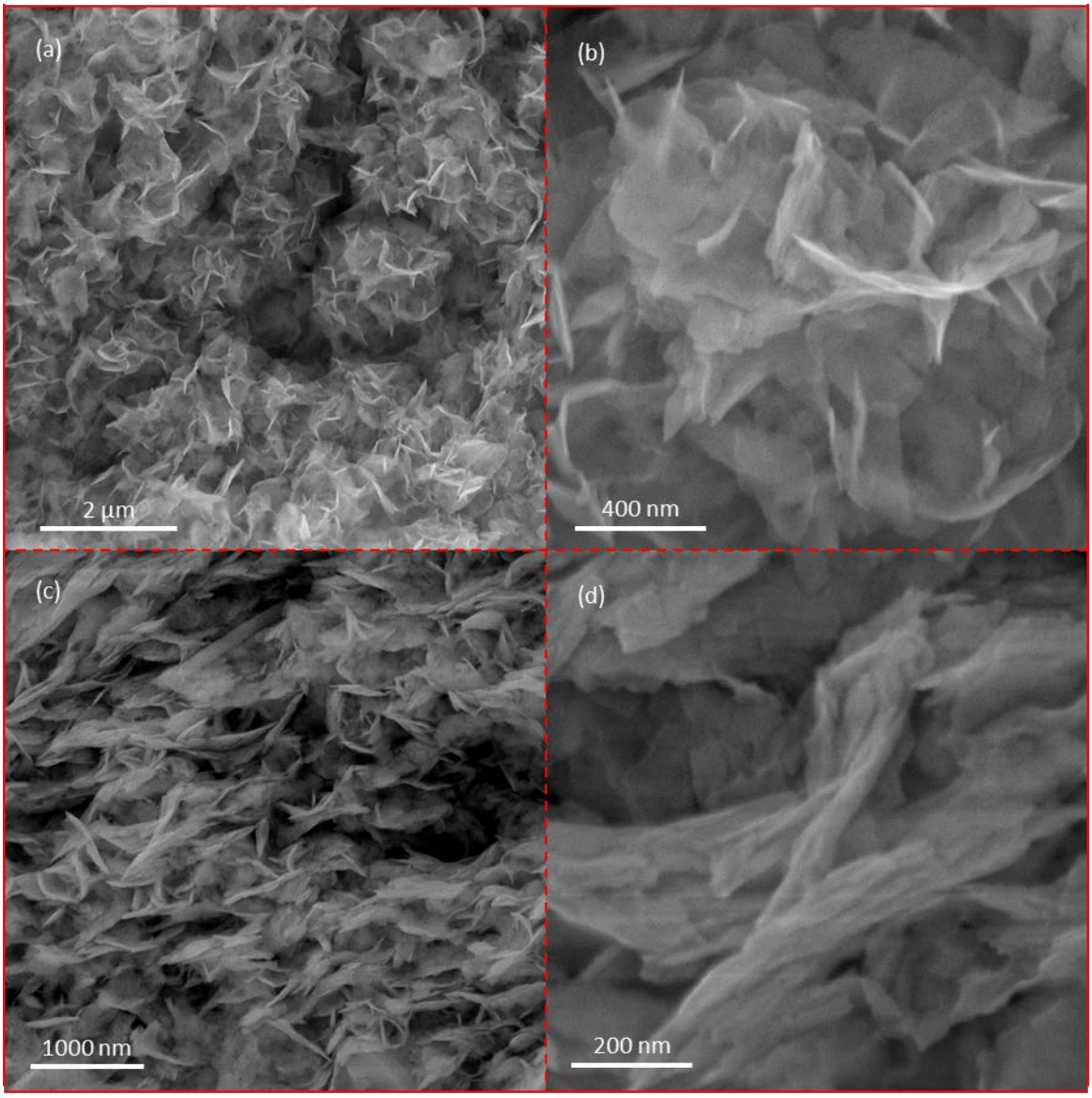

Fig. S14 SEM images of (a, b) BiOI-P123 and (c, d) BiOBr-P123

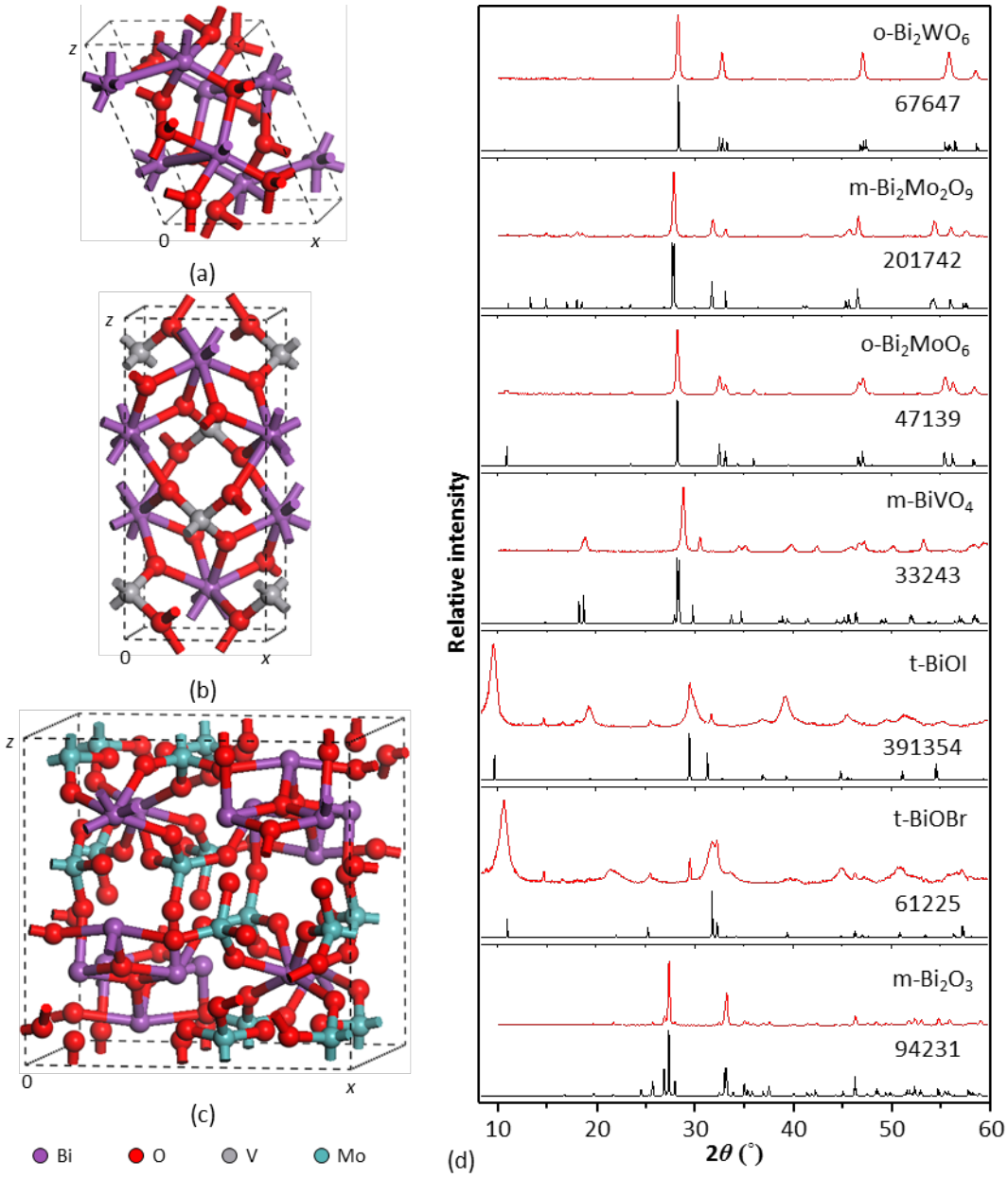

Fig. S15 Representation of the crystal structures of (a) m-Bi_2O_3, (b) m-$BiVO_4$, and (c) m-$Bi_2Mo_2O_9$, (d) experimental XRD patterns of Bi_2O_3, BiOX, and $Bi_xM_yO_z$ referenced to simulated patterns.

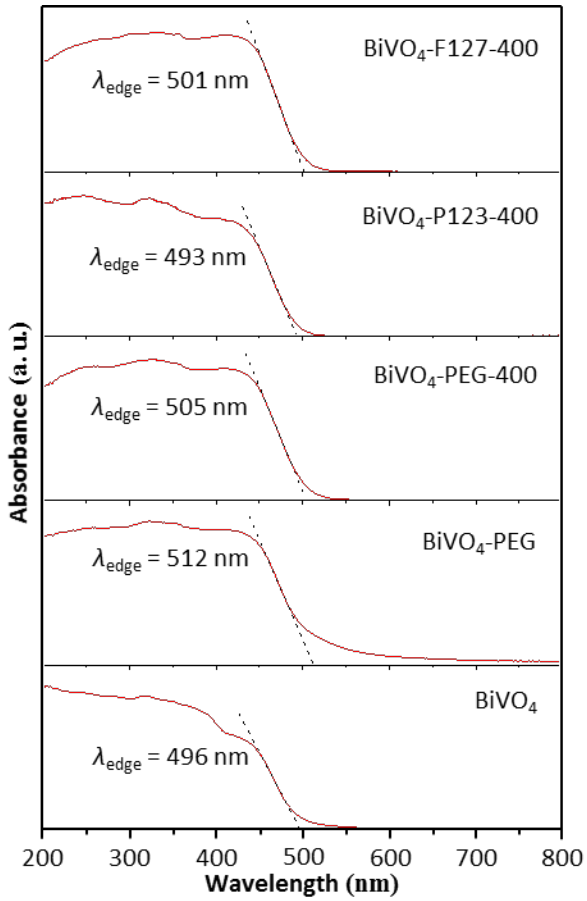

Fig. S16 DRS spectra of $BiVO_4$, $BiVO_4$-PEG, and $BiVO_4$-polymer-400.

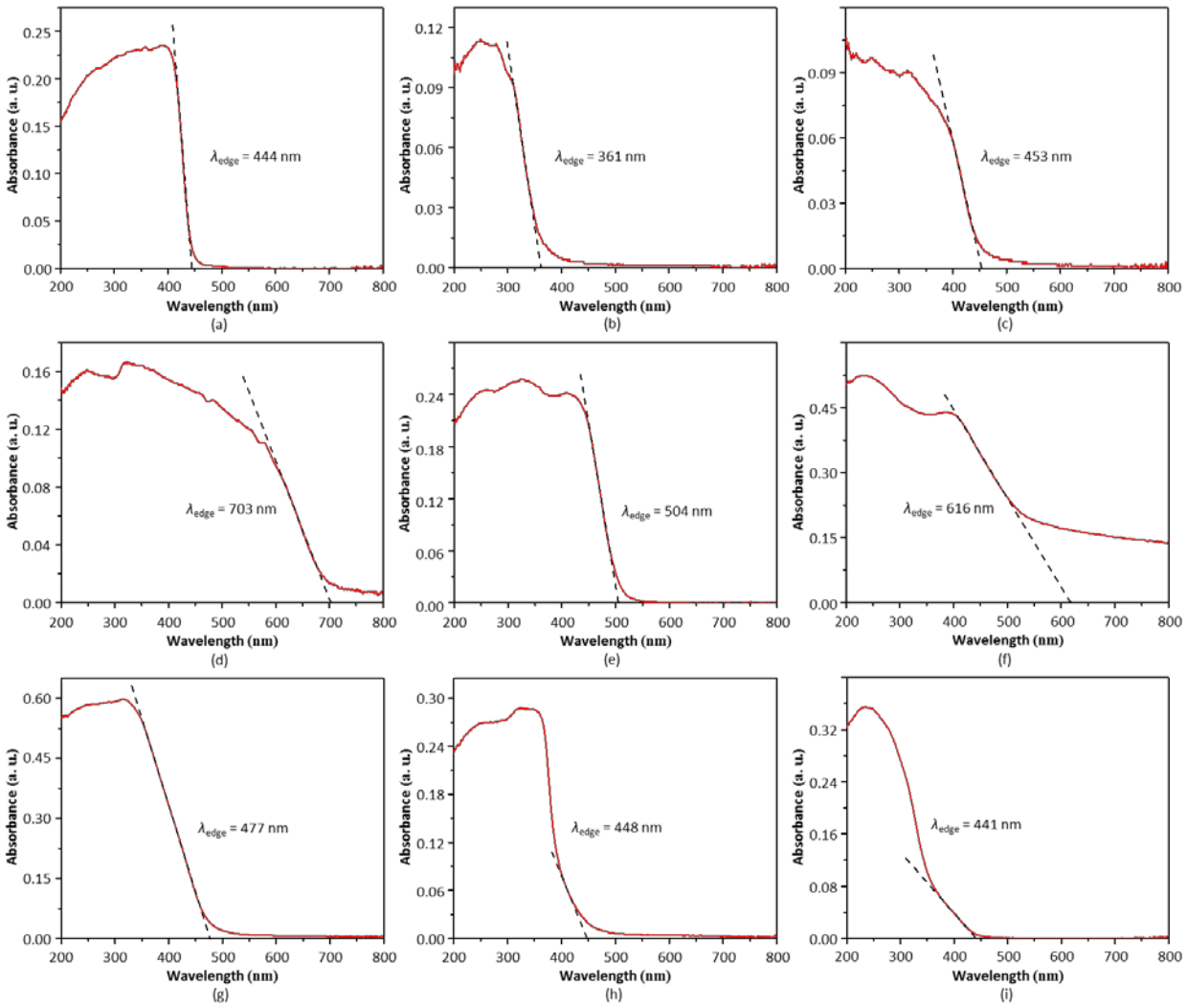

Fig. S17 DRS spectra of (a) Bi_2O_3-PEG-350, (b) BiOCl-PEG, (c) BiOBr-PEG, (d) BiOI-PEG, (e) $BiVO_4$-PEG-400, (f) $Bi_xCr_xO_z$-PEG-400, (g) Bi_2MoO_6-PEG-400, (h) $Bi_2Mo_2O_9$-PEG-400, and (i) Bi_2WO_6-PEG-400.

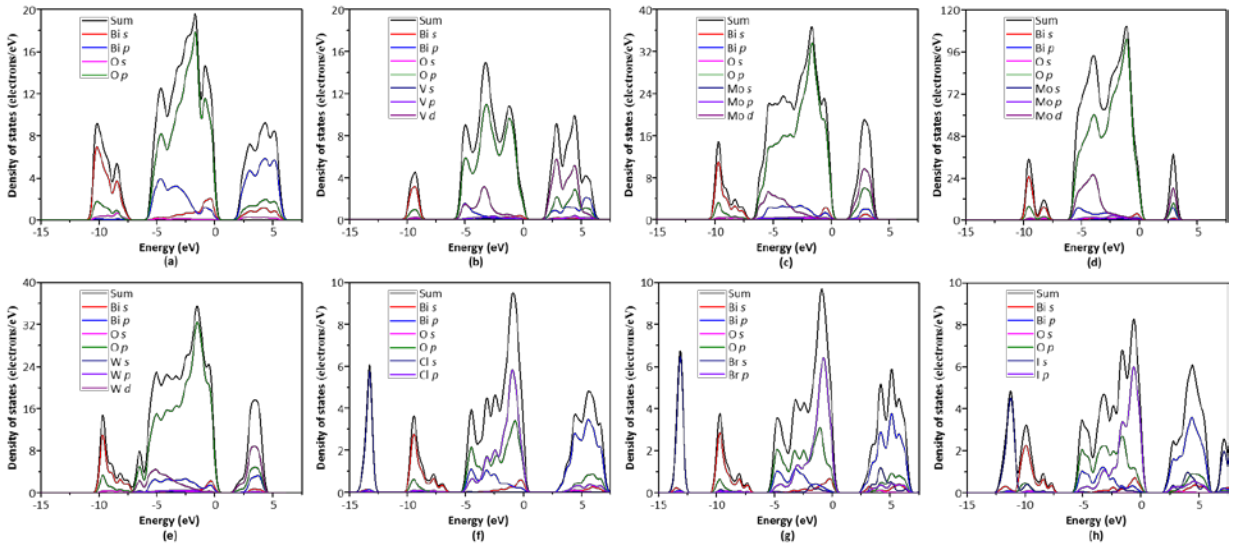

Fig. S18 Plots of density of states of (a) m-Bi_2O_3, (b) m-$BiVO_4$, (c) o-Bi_2MoO_6, (d) m-$Bi_2Mo_2O_9$, (e) o-Bi_2WO_6, (f) t-BiOCl, (g) t-BiOBr, and (h) t-BiOI.

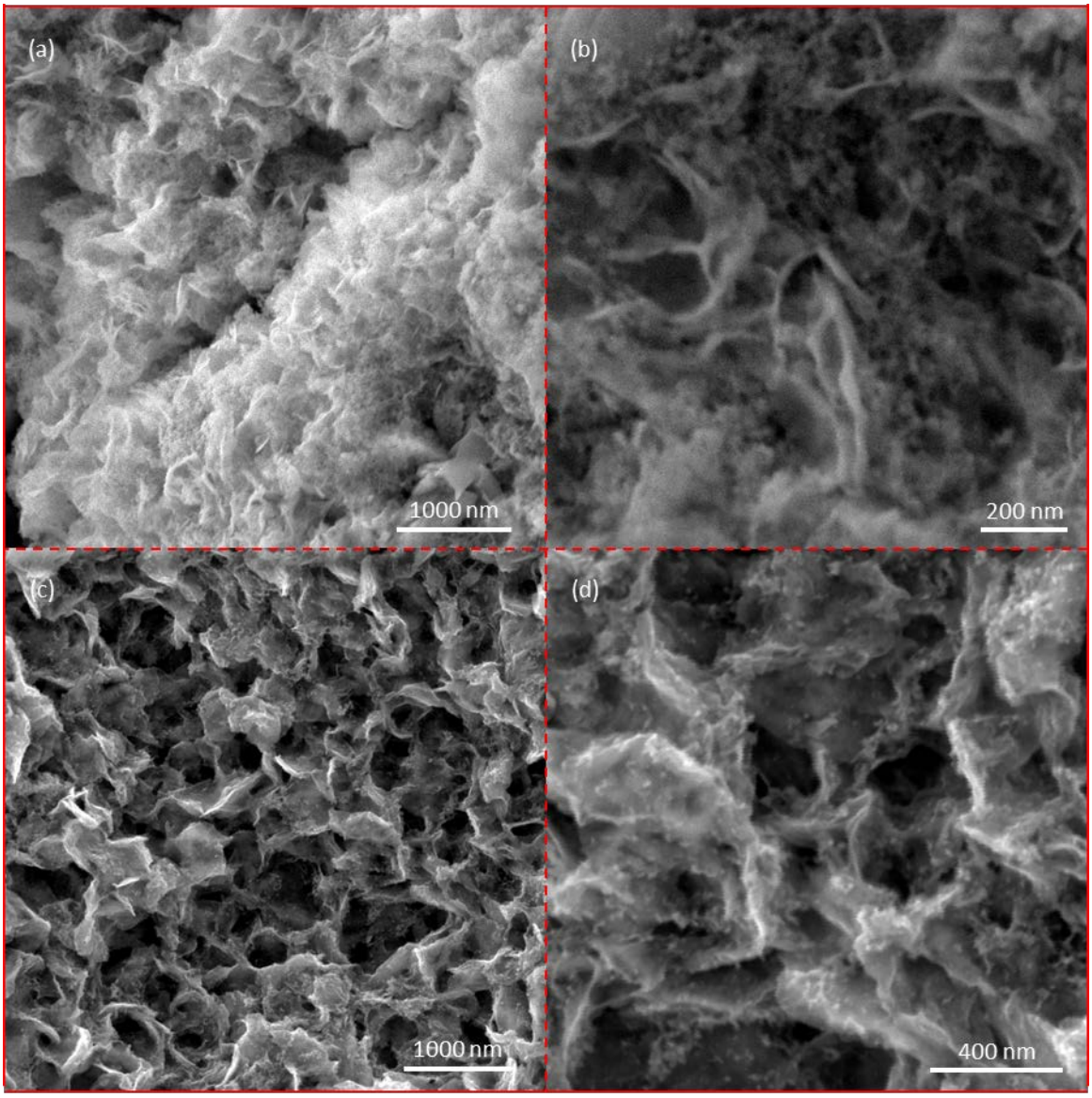

Fig. S19 SEM images of (a, b) $BiVO_4$-BiOI-PEG and (c, d) $BiVO_4$-BiOBr-BiOI-PEG.

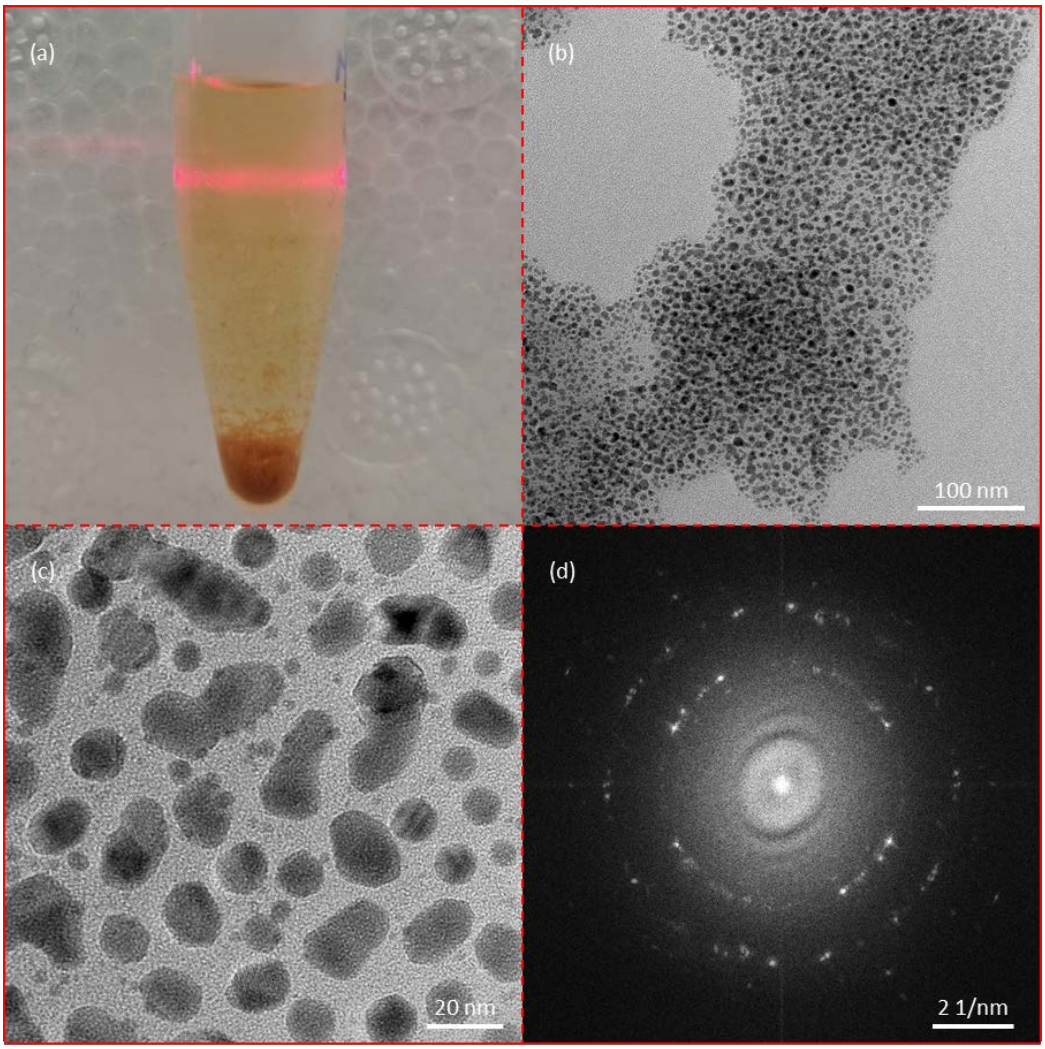

Fig. S20 (a) Photograph of the copper oxide suspension showing Tyndall effect, (b, c) TEM images of the precipitate in (a), (d) FFT of (c).

References

1 S. J. Clark, M. D. Segall, C. J. Pickard, P. J. Hasnip, M. I. Probert, K. Refson and M. C. Payne, *Z. Kristallogr.*, 2005, **220**, 567-570.

2 J. P. Perdew, A. Ruzsinszky, G. I. Csonka, O. A. Vydrov, G. E. Scuseria, L. A. Constantin, X. Zhou and K. Burke, *Phys. Rev. Lett.*, 2008, **100**, 136406.

3 B. G. Pfrommer, M. Côté, S. G. Louie and M. L. Cohen, *J. Comput. Phys.*, 1997, **131**, 233-240.